Distribution-free P-box processes based on translation theory: definition and simulation

Matthias G.R. Faes[1], Matteo Broggi[b], Guan Chen[b,f], Kok-Kwang Phoon[d], Michael Beer[b,c,e]

[a] *TU Dortmund University, Chair for Reliability Engineering. Leonhard-Euler-Straße 5, 44227 Dortmund, Germany. Email: matthias.faes@tu-dortmund.de*

[b] *Institute for Risk and Reliability, Leibniz Universität Hannover, Callinstr. 34, 30167 Hannover, Germany*

[c] *Institute for Risk and Uncertainty and School of Engineering, University of Liverpool, Peach Street, Liverpool L69 7ZF, UK*

[d] *Singapore University of Technology and Design, Singapore*

[e] *International Joint Research Center for Resilient Infrastructure & International Joint Research Center for Engineering Reliability and Stochastic Mechanics, Tongji University, Shanghai, P.R. China*

[f] *State Key Laboratory of Water Resources and Hydropower Engineering Science, Institute of Engineering Risk and Disaster Prevention, Wuhan University, Wuhan 430072, P.R. China*

Abstract

Typically, non-deterministic models of spatial or time dependent uncertainty are modelled using the well-established random field framework. However, while tailored for exactly these types of time and spatial variations, stochastic processes and random fields currently have only limited success in industrial engineering practice. This is mainly caused by its computational burden, which renders the analysis of industrially sized problems very challenging, even when resorting to highly efficient random field analysis methods such as EOLE. Apart from that, also the methodological complexity, high information demand and rather indirect control of the spatial (or time) variation has limited its cost-benefit potential for potential end-users. This data requirement was recently relaxed by some of the authors with the introduction of imprecise random fields, but so far the method is only applicable to parametric p-box valued stochastic processes and random fields. This paper extends these concepts by expanding the framework towards distribution-free p-boxes. The main challenges addressed in this contribution are related to both the non-Gaussianity of realisations of the imprecise random field in between the p-box bounds, as well as maintaining the imposed auto-correlation structure while sampling from the p-box. Two case studies involving a dynamical model of a car suspension and the settlement of an embankment are included to illustrate the presented concepts.

Keywords: Stochastic process; imprecise probability; probability box; random field; scarce data

1. Introduction

1.1. General rationale

Stochastic processes are applied and studied in various domains, reaching from engineering [1] to financial economics, to represent stochastic quantities that vary over time- and/or space [2]. However,

due to the theoretical and computational difficulties, usually these processes are assumed to be Gaussian, which might not always be a truthful representation of reality [10]. Furthermore, the definition of a stochastic process requires the rigorous description of the governing distribution function. This includes selecting the appropriate distribution family as well as the governing hyper-parameters. In practice, an accurate definition of these quantities might not be possible due to limitations on the available data (quantity of the data, corrupted or missing data, etc.), but also conflicting sources of information (e.g., expert opinions). Recently introduced approaches based on Bayesian compressed sensing alleviate this problem (see e.g., [3, 4] by making the estimated stochastic process robust to missing data, even when these processes are non-Gaussian and have an unknown non-stationary auto-correlation function [5]. Furthermore, also de-trending is not required in these cases [5]. In [6], these methods were extended to also account for the general case of multivariate, uncertain, unique, sparse, incomplete spatial data (denoted MUSIC-X by the authors).

As a possible alternative pathway to account for low data availability is to resort to the more general framework of imprecise probabilities [7]. According to this framework, epistemic uncertainty that results from data deficiencies are taken explicitly into account in the analysis. In the context of stochastic processes, parametric p-box valued stochastic processes have been introduced in e.g., [13], [14] and [15]. However, such approaches still require the definition of a (Gaussian) distribution family, which is not always possible. This paper aims to go further than the available methods for simulating from imprecise stochastic processes by introducing a type of distribution-free p-box stochastic process. Such process is obtained by applying an interval-valued translation map to a standard normal Gaussian stochastic process. As such, a distribution-free p-box stochastic process is obtained. Two examples are included to illustrate the definition and propagation of these structures. The paper is constructed as follows: the remainder of this section retakes some important concepts concerning the definition and simulation of non-Gaussian stochastic processes; Section 3 introduces the approach for defining distribution-free p-box processes; Section 4 briefly discusses a double-loop approach to propagate these structures; Section 5 and Section 6 provide two case studies as illustration of the approach; Section 7 lists the conclusions of the work.

2. Background theory

This section retakes some background theory on non-Gaussian stochastic processes to facilitate the understanding of the developments presented further in the paper. Specifically, the general theory behind stochastic processes is reproduced for the sake of unifying some definitions and highlighting some key concepts. Further, translation theory is explained in detail since the ensuing developments are largely

based on this concept.

2.1. Stochastic processes

A finite-dimensional stochastic process $x(t,\omega)$ describes a set of correlated random variables $x(\omega)$, which are assigned to a countable number n_t of locations $t \in \Omega_d$ in the model domain $\Omega_d \subset \mathbb{R}^d$ with dimension $d \in \mathbb{N}$. Note that Ω_d may comprise both space and/or time dimensions. Each random variable $x(\omega) : (\Omega, \varsigma, P) \mapsto \mathbb{R}$ as such maps from a complete probability space to the real domain, with $\omega \in \Omega$ a coordinate in sample space Ω and ς the sigma-algebra. This condition holds as long as $x(t,\omega) \in \mathcal{L}^2(\omega, P)$, with $\mathcal{L}^2(\omega, P)$ the Hilbert space of second-order random variables (i.e., finite variance). For a given event $\omega_i \in \Omega$, the corresponding $x(t,\omega_i)$ is a realization of the stochastic process. A stochastic process is considered Gaussian if the distribution of $(x(t_1,\omega), x(t_2,\omega), \ldots, x(t_{n_t},\omega))$, with $n_t \in \mathbb{N}$, is jointly Gaussian $\forall t \in \Omega_d$. In this case, $x(t,\omega)$ is completely described by its mean function $\mu_x(t) : \Omega_d \mapsto \mathbb{R} = E_\omega[x(t,\omega)]$ and its auto-covariance function $\mathbf{C}_{xx}(\tau) : \Omega_d \times \Omega_d \mapsto \mathbb{R}$, given by $\mathbf{C}_{xx}(\tau) = E_\omega[(x(t,\omega) - \mu_x(t)), (x(t',\omega) - \mu_x(t))]$ [2]. In the remainder of the paper, uni-variate scalar stochastic processes (i.e., $\Omega \in \mathbb{R}^1$) are considered for the sake of conciseness of notation. Note that the concepts explained in this paper scale straightforwardly to multidimensional random fields as well (i.e., random fields defined over $\mathbb{R}^d, d > 1$, with the only difference that t and τ become vector-valued. Also the extension towards multi-variate and multi-index random fields should not pose too many challenges, since the concepts upon which the methods are built (i.e., translation theory) are well-understood in this context (see e.g., [34]). An in-depth discussion of such extension is left for further work.

Generally, when applying stochastic processes in an engineering context, for instance to represent a spatially uncertain input quantity of a finite element model, the process has to be discretized over Ω_d. In this context, the Karhunen-Loève expansion is a very powerful tool to represent stochastic processes [8]. Specifically, following the Karhunen-Loève (KL) series expansion, a stochastic process $x(t,\omega)$ is represented as:

$$x(t,\omega) = \mu_x(t) + \sigma_x \sum_{i=1}^{\infty} \sqrt{\lambda_i} \boldsymbol{\psi}_i(t) \xi_i(\omega), \tag{1}$$

with σ_x the standard deviation of the random process and where the quantities $\lambda_i \in (0, \infty)$ and $\boldsymbol{\psi}_i(t) : \Omega_d \mapsto \mathbb{R}$ are respectively the eigenvalues and eigenfunctions of the continuous, bounded, symmetric and positive (semi-)definite auto-correlation function $\boldsymbol{\rho}_{xx}(\tau) : \Omega_d \times \Omega_d \mapsto [0, 1]$, in accordance with Mercer's theorem:

$$\boldsymbol{\rho}_{xx}(\tau) = \sum_{i=1}^{\infty} \lambda_i \boldsymbol{\psi}_i(t) \boldsymbol{\psi}_i(t'), \tag{2}$$

These quantities are in practice obtained by solving the homogeneous Fredholm integral equation of

the second kind:

$$\int_{\Omega_d} \boldsymbol{\rho}_{xx}(\tau)\boldsymbol{\psi}_i(t')dt' = \lambda_i \boldsymbol{\psi}_i(t), \tag{3}$$

where $t' = t + \tau$ for which many efficient discretization schemes exist [9]. Since $\boldsymbol{\rho}_{xx}(\tau)$ is bounded, symmetric and positive semi-definite, and furthermore in most practical cases can be assumed positive definite, these eigenvalues λ_i are non-negative and the eigenfunctions $\boldsymbol{\psi}_i(t)$ satisfy the following orthogonality condition:

$$\langle \boldsymbol{\psi}_i(t), \boldsymbol{\psi}_j(t) \rangle = \int_{\Omega_d} \boldsymbol{\psi}_i(t)\boldsymbol{\psi}_j(t)dt = \delta_{ij} \tag{4}$$

with δ_{ij} the Kronecker delta and $\langle \cdot, \cdot \rangle : \Omega_d \times \Omega_d \mapsto \mathbb{R}$ an inner product space. Hence, the eigenfunctions form a complete orthogonal basis on an $\mathcal{L}_2$ Hilbert space. In this case, the series expansion in Eq. 2 can be shown to be optimally convergent [8].

The variables $\xi_i(\omega), i = 1, \ldots, \infty$, introduced in Eq. 1, are uncorrelated random variables, which are determined according to:

$$\xi_i(\omega) = \frac{1}{\sqrt{\lambda_i}} \int_{\Omega_d} \left[x(t,\omega) - \mu_x(t)\right] \boldsymbol{\psi}_i(t)dt, \tag{5}$$

which can be shown to be independent standard normally distributed in the case of a Gaussian random process. For practical reasons, the infinite series expansion in Eq. 1 is usually truncated after a finite number of terms $n_{KL} \in \mathbb{N}$:

$$x(t,\omega) = \mu_x(t) + \sigma_x \sum_{i=1}^{n_{KL}} \sqrt{\lambda_i}\boldsymbol{\psi}_i(t)\xi_i(\omega), \tag{6}$$

where n_{KL} should be selected such that a well-chosen variance error metric is minimized [11] .

In the context of applying stochastic processes in an imprecise probabilistic context, the Gaussian-assumption is no longer generally valid. This has several implications for their discretization. For non-Gaussian processes, the $\xi_i(\omega), i = 1, \ldots, n_{KL}$ represented in Eq. 5 are non-Gaussian too and their distribution needs to be solved for explicitly. Furthermore, in this case, the corresponding random variables $\xi_i(\omega)$ may exhibit higher order dependencies that are difficult to quantify [10]. Finally, Eq. 5 reveals that the distribution of $\xi_i(\omega)$ depends on sample path realisations $x(t,\omega)$ of the stochastic process, and hence, iterative methods such as presented by [11] need to be applied. Alternatively, also translation theory as introduced by Grigoriu [21] provides a viable approach towards simulating from (strongly) non-Gaussian stochastic processes.

2.2. Translation stochastic processes

Translation process theory, as introduced by Grigoriu [21], provides a different pathway for the simulation of non-Gaussian stochastic processes. Specifically, a Gaussian stochastic process $\eta(t,\omega)$ with autocorrelation function $\rho_{xx}(\tau)$ is transformed using a nonlinear transformation into a non-Gaussian

process $x(t,\omega)$. This is formally expressed as:

$$x(t,\omega) = F_X^{-1} \circ \Phi(\eta(t,\omega)) = g(\eta(t,\omega)), \tag{7}$$

with $g := F_X^{-1} \circ \Phi$ the so-called translation mapping, F_X^{-1} the inverse of the target non-Gaussian cumulative distribution function (CDF) that represents the distribution of the non-Gaussian stochastic process and Φ the marginal standard normal CDF, i.e., $\Phi(\eta) = P(\eta(t,\omega) < \eta)$.

It can be shown (see [21]) that the mean μ_x, variance σ_x^2 and correlation function $r_{xx}(\tau)$ of $x(t,\omega)$ have closed-form expressions, that are given respectively by:

$$\mu_x = E_\eta[x(t,\omega)] = E_\eta[g(\eta(t,\omega))] = \int_{-\infty}^{\infty} g(\eta)\phi(\eta)d\eta \tag{8}$$

$$\sigma_x^2 = E_\eta[x(t,\omega) - \mu_x]^2 = \int_{-\infty}^{\infty} (g(\eta) - \mu_x)^2\phi(\eta)d\eta \tag{9}$$

$$r_{xx}(\tau) = E[x(t,\omega) - \mu_x]E[x(t+\tau,\omega) - \mu_x] = \int_{-\infty}^{\infty}\int_{-\infty}^{\infty} (g(\eta_1) - \mu_x)(g(\eta_2) - \mu_x)\phi(\eta_1, \eta_2, \rho_{xx}(\tau))dydz \tag{10}$$

with $\phi(\eta_1, \eta_2, \rho_{xx}(\tau))$ the density of a bivariate standard Gaussian vector with correlation coefficient $\rho_{xx}(\tau)$, given by:

$$\phi(\eta_1, \eta_2, \rho_{xx}(\tau)) = \frac{1}{\sqrt{2\pi(1-\rho_{xx}(\tau)^2)}} \exp -\frac{\eta_1^2 + \eta_2^2 - 2\eta_1\eta_2\rho_{xx}(\tau)}{2(1-\rho_{xx}(\tau))^2} \tag{11}$$

These equations can be readily solved by standard numerical quadrature schemes. Furthermore, it can be shown that the forward transformation of a Gaussian process to a non-Gaussian process is always possible ([21]).

On the other hand, given a non-Gaussian $r_{xx}(\tau)$, it is not always possible to determine the corresponding Gaussian autocorrelation $\rho_{xx}(\tau)$ that, when transformed, yields $r_{xx}(\tau)$ [21]. This happens when either the inverse of Eq. 10 yields an autocorrelation function that is not positive semi-definite, or when the normalized autocorrelation $\xi(\tau)$ has values that lie outside of the admissible range $[\xi^{min}(\tau), \xi^{max}(\tau)]$ which can be found by setting $\rho_{xx}(\tau)$ to respectively 1 and -1 in Eq. 10 [22]. In literature, iterative methods have been introduced to find the closest approximation of $r_{xx}(\tau)$ that is an admissible autocorrelation function (see e.g., [12]).

3. P-box stochastic processes

In practical engineering cases, it is not always possible to define a precise distribution function $F_X(x)$ to construct the non-Gaussian stochastic process. In this context, p-boxes can provide a valuable tool to

represent the uncertainty an analysist has on the specification of the appropriate distribution function (see [16] for a recent review on computational methods). This section introduces p-box-valued stochastic processes.

As a practical example on how such a P-box can be established in geotechnical analysis, consider Figure 1. This figure shows a normal probability plot for the Rock Mass Rating (RMR) values at the Izmir subway site (taken from [19]). As may be seen, the 95% probability bounds corresponding to a performed normality fit indicate that the estimation of the Normal distribution with these data is the most accurate around the mean value, and that the uncertainty of the fit increases towards the tails of the distribution. This particular point was also made by Ching et al., who showed that statistical uncertainty for random field parameters can be very big due to strong data constraints in geotechnical engineering [20]. In this case, one might consider to rather make calculations with the bounds provided by the confidence interval, and all therein included distributions, rather than with the precise Normal estimate, as it relaxes the quite restricting Normality assumption. Indeed, by considering a set of distributions, a more robust and natural approach to deal with the existing uncertainties is followed, yielding more objective estimates. Similar scarce data examples can be found in multiple engineering applications, ranging from modelling wind loads on buildings, predicting earthquakes, or dealing with highly advanced engineered materials such as encountered in Additive Manufacturing.

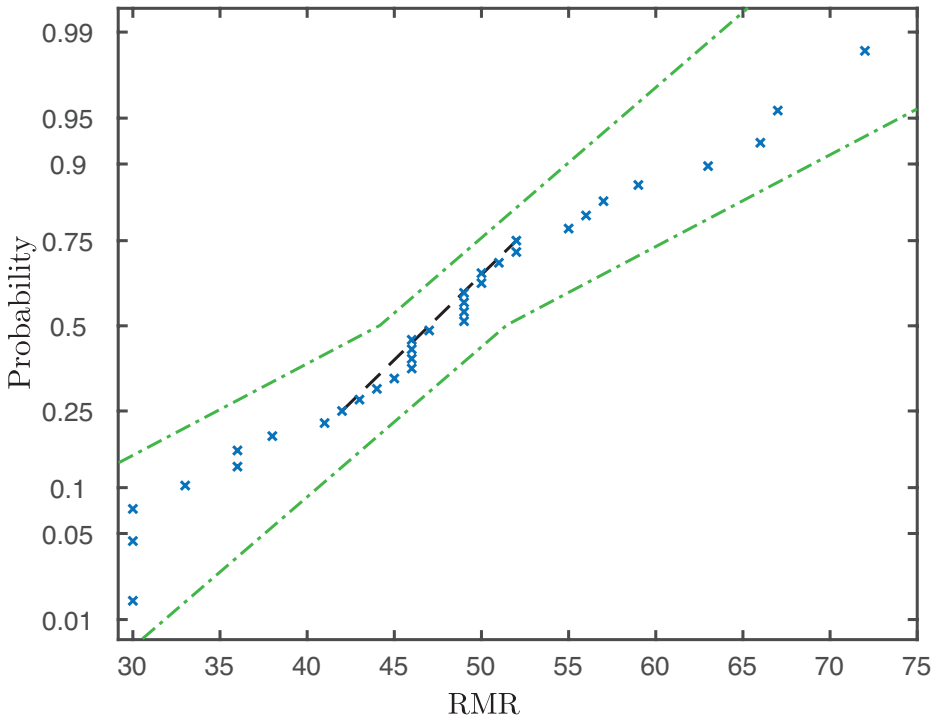

Figure 1: Normal probability plot, including the confidence interval bounds for the Rock Mass Rating data, taken from the Izmir subway site (taken from [19]). The black dashed line indicates the fitted normal distribution, the green dash-dotted lines indicate the confidence interval on this fit.

A scalar distribution-free p-box is usually described by a lower CDF $\underline{F}_X \in \mathbb{F}$ and an upper CDF $\overline{F}_X \in \mathbb{F}$, where $\mathbb{F}$ expresses the the set of all CDFs on $\mathbb{R}$. They are collected as a pair $\left[\underline{F}_X, \overline{F}_X\right]$ which yields a set of possible CDFs via $\underline{F}_X(x) \leq F_X(x) \leq \overline{F}_X(x),\ x \in \mathbb{R}$. A distribution-free p-box as such corresponds to defining a lower probability $\underline{P}$ and upper probability $\overline{P}$ on events $\{X \leq x\} = (-\infty, x]$, i.e., $\underline{P}(X \leq x) = \underline{F}_X(x)$ and $\overline{P}(X \leq x) = \overline{F}_X(x)$ for $x \in \mathbb{R}$, which define a credal set of probability measures. In case additional information on the uncertainty is available, constraints on the p-box can be enforced. For instance, if the (class of) distribution functions $\mathcal{F}$ is known, the set of possible CDFs $\{F_X(\cdot, \boldsymbol{\theta}) \in \mathcal{F} \mid \boldsymbol{\theta} \in D_{\boldsymbol{\theta}}\}$ can be defined conditional on a vector of hyper-parameters $\boldsymbol{\theta}$. Since this is a special case of the distribution-free p-box, the following discussion on distribution-free p-box stochastic is equally applicable. An important side-note should be made with respect to distribution-free p-boxes. Due to the relaxed constraints on the set of admissible CDFs, generally, also non-physical distribution functions are explicitly modelled in the p-box. It should be noted that developments in this context have been made, focusing on imposing some constraints on the realisations within the distribution-free p-box [18, 17].

As explained in Section 2, a (precise) stochastic process $x(t, \omega)$ can be considered as a collection of n_t correlated random variables distributed throughout the model domain Ω_d. Imprecise stochastic processes $\hat{x}(t, \omega)$ can be regarded as a natural extension of this idea, where for each discrete location $t_i \in \Omega_d$, a scalar p-box is defined. However, since all $x(t_i, \omega),\ i = 1, \ldots, n_t$ are correlated according to $\rho_{xx}(\tau)$, these scalar p-boxes also are correlated to each other. This observation complicates the analysis of distribution-free imprecise stochastic processes significantly, since the direct simulation from a set of correlated distribution-free p-boxes is far from trivial from both a theoretical as well as from a numerical point of view. Furthermore, since distribution-free p-boxes are considered, also non-Gaussian processes are inherently included in the imprecise stochastic description.

A potential solution to this issue is to start from a precise standard normal Gaussian stochastic process $\eta(t, \omega)$ with predefined correlation function $\rho_{xx}(\tau)$ and pass this representation through an imprecisely defined translation map which is defined as:

$$\hat{x}(t, \omega) = \left[\underline{F}_X^{-1}, \overline{F}_X^{-1}\right] \circ \Phi(\eta(t, \omega)), \tag{12}$$

which can be further expanded as:

$$\hat{x}(t, \omega) = \left[\underline{F}_X^{-1}, \overline{F}_X^{-1}\right] \circ \Phi\left(\sum_{i=1}^{n_{KL}} \sqrt{\lambda_i} \boldsymbol{\psi}_i(t) \xi_i(\omega)\right), \tag{13}$$

where $\Phi\left(\sum_{i=1}^{n_{KL}} \sqrt{\lambda_i} \boldsymbol{\psi}_i(t) \xi_i(\omega)\right)$ represents a re-scaling of $\eta(t, \omega)$ to the interval $[0, 1]$. Since a CDF is

by definition a monotonic function, i.e., $F_X(x_1) < F_X(x_2) \iff x_1 < x_2$, the bounds of $\hat{x}(t,\omega)$ are determined by $\left[\underline{F}_X^{-1}, \overline{F}_X^{-1}\right]$. It can be noted that the outer part of the interval-valued translation map, i.e., $\left[\underline{F}_X^{-1}, \overline{F}_X^{-1}\right]$ in effect represents the inverse of a distribution-free p-box. As such, the interval-valued translation map at first scales $\eta(t,\omega)$ to $[0,1]$, after which a set-valued transformation is applied to transform this stochastic process into an imprecise stochastic process according to the p-box that is bounded by $\left[\underline{F}_X^{-1}, \overline{F}_X^{-1}\right]$.

In essence, for each x, the p-box $\left[\underline{F}_X, \overline{F}_X\right]$ provides an interval $\left[\underline{F}_X(x), \overline{F}_X(x)\right]$. Therefore, $\left[\underline{F}_X^{-1}, \overline{F}_X^{-1}\right] \circ \Phi$ analogously represents an interval-valued mapping of each realisation of $\eta(t,\omega)$. As such, each realisation of the stochastic process $\eta(t,\omega_j)$, corresponding to the event ω_j is translated towards an interval process that is consistent with the bounds on the CDF (due to the monotonicity of the CDF), and which is given as:

$$x^I(t,\omega_j) = \left[\underline{F}_X^{-1}, \overline{F}_X^{-1}\right] \circ \Phi\left(\sum_{i=1}^{n_{KL}} \sqrt{\lambda_i}\boldsymbol{\psi}_i(t)\xi_i(\omega_j)\right), \tag{14}$$

with the lower bound given as:

$$\underline{x}(t,\omega_j) = \overline{F}_X^{-1} \circ \Phi\left(\sum_{i=1}^{n_{KL}} \sqrt{\lambda_i}\boldsymbol{\psi}_i(t)\xi_i(\omega_j)\right), \tag{15}$$

and the upper bound defined as:

$$\overline{x}(t,\omega_j) = \underline{F}_X^{-1} \circ \Phi\left(\sum_{i=1}^{n_{KL}} \sqrt{\lambda_i}\boldsymbol{\psi}_i(t)\xi_i(\omega_j)\right). \tag{16}$$

It should be noted that this is not an explicit interval process, i.e., an interval process that is represented as a series expansion with interval-valued coefficients as described in [23], since the interval-valued nature in this process stems from the mapping that is performed on a single realisation of the precise Gaussian process, rather than from a series expansion with interval-valued weights. As such, typically applied interval propagation methods, as described in [24], cannot be applied to propagate this interval process in a straightforward way. Furthermore, the auto-dependence function of realisations within this interval process becomes inter-valued too. Intermediate realisations of $x^k(t,\omega_j) \in x^I(t,\omega_j)$ can be generated by drawing admissible CDFs $(F_X^k)^{-1} \in \left[\underline{F}_X^{-1}, \overline{F}_X^{-1}\right]$. For reasons of clarity, the explanation of a possible procedure to do so is deferred to a later section. For more information about interval processes (and -fields), the reader is referred to the work of [25], [26] or [27], who all defined interval processes according to different formalisms.

Conversely, when collecting all $x^k(t,\omega)$, that corresponds to a certain realisation of the p-box $(F_X^k)^{-1} \in [\underline{F}_X^{-1}, \overline{F}_X^{-1}]$, this becomes again a precise random process, the properties of which can be computed by

virtue of translation process theory as:

$$\mu_{x^k(t,\omega)} = \int_{-\infty}^{\infty} (F_X^k)^{-1} \circ \Phi(\eta)\phi(\eta)d\eta \tag{17}$$

$$\sigma^2_{x^k(t,\omega)} = \int_{-\infty}^{\infty} ((F_X^k)^{-1} \circ \Phi(\eta) - \mu_{x^k(t,\omega)})^2\phi(\eta)d\eta \tag{18}$$

$$r_{x^k}(\tau) = \int_{-\infty}^{\infty}\int_{-\infty}^{\infty} ((F_X^k)^{-1} \circ \Phi(\eta_1) - \mu_{x^k(t,\omega)})((F_X^k)^{-1} \circ \Phi(\eta_2) - \mu_{x^k(t,\omega)})\phi(\eta_1, \eta_2, \rho_{xx}(\tau))d\eta_1 d\eta_2 \tag{19}$$

with $\phi(\eta_1, \eta_2, \rho_{xx}(\tau))$ as defined in Eq. (11). Note that this random process is stationary in case the underlying Gaussian process is stationary since it is mapped through a precise $(F_X^k)^{-1}$. Evidently every $(F_X^k)^{-1}$ will yield a random process with generally different central moments for every $(F_X^k)^{-1} \in [\underline{F}_X^{-1}, \overline{F}_X^{-1}]$.

Based on the preceding discussion, it can be seen that an imprecise stochastic process can jointly be regarded as a stochastic collection of interval processes as well as as a credal set of stochastic processes. Since each stochastic realisation of the imprecise stochastic process is an interval process, and vice versa, each realisation within the p-box corresponds to a stochastic process, also the mean of the corresponding imprecise process is interval-valued. Due to the monotonicity of the translation map, this mean is formally given as:

$$\mu_x^I = [\underline{\mu}_x, \overline{\mu}_x] = \left[E_\omega\left[\underline{x}(t,\omega)\right], E_\omega\left[\overline{x}(t,\omega)\right]\right]. \tag{20}$$

These bounds can be computed in a straightforward manner by invoking Eq. 17 twice: once on the ensemble of lower bounds and once on the ensemble of upper bounds. As an illustration of these concepts, consider the example in Figure 2. This figure shows two stochastic realisations of the precise zero-mean Gaussian stochastic process, as well as their transformation into two realisations of the distribution-free p-box random process, which manifest themselves in the shape of two interval processes. From this figure, it can also be seen that the collection of all upper bounds of these interval processes, denoted $\overline{x}(t,\omega)$, represent a stochastic process that has $\overline{F}_X(x)$ as a distribution. The same obviously holds for the lower bound, as well as any intermediate realisation $(F_X^k)^{-1} \in \left[\underline{F}_X^{-1}, \overline{F}_X^{-1}\right]$.

It should further be noted that the auto-correlation function of $x^I(t,\omega)$, being $r_{xx}(\tau)$ also has become an interval-valued function that may be modelled as an interval process due to the interval-valued translation map. This might have important implications for structural dynamical problems, where the match of a dominant frequency of the loading process might interfere with a natural frequency of the structure. The detailed treatment of this issue and a potential solution hereto however fall outside the scope of this paper.

As a final comment, Figure 1 hints at a possible, very straighforward, approach to infer the bounds

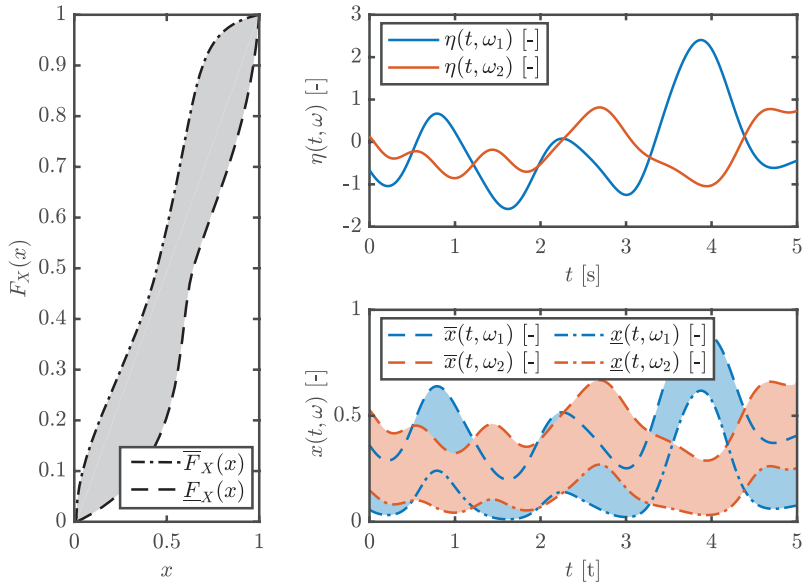

Figure 2: Illustration of the transformation of two stochastic realisations of the precise zero-mean Gaussian stochastic process into two realisations of the distribution-free p-box random process, which manifest themselves in the shape of two interval processes.

of the p-box valued translation map based on a small data-set. As is clear in the Figure, the confidence bounds in the normality fit of rock data are clearly expanding towards the tails of the distribution. One possible approach could be to use those confidence bounds as the bounds of the p-box to ensure robustness of the results with respect to the (lack of) confidence in the normal fit. Of course, also more elaborate schemes can be imagined, for instance based on Kolmogorov-Smirnov bounds or robust Bayesian analysis. This is however left for future work.

4. Propagation of distribution-free imprecise stochastic processes

Usually, an analyst who is confronted with imprecise probabilistic model quantities is concerned with finding the bounds on some probabilistic measure $\mathcal{P}$ of the model's responses of interest. In case a precise density function $f_{\boldsymbol{X}}$ is known, the n^{nt} central moment of the model's response $E_{\boldsymbol{y}}[Y^n]$ or the probability of failure p_F is determined by solving an integral equation of the following form:

$$\mathcal{P}(F_X^k) = \int_{\mathbb{R}^{n_x}} \mathcal{H}\left(\boldsymbol{x} \,\middle|\, F_X^k\right) f_{\boldsymbol{X}}^k(\boldsymbol{x})\,\mathrm{d}\boldsymbol{x}, \tag{21}$$

where $\mathcal{P}$ denotes, depending on the context, the n^{th} central moment of the model's response $E_{\boldsymbol{y}}[Y^n]$ or the probability of failure p_F. In case $\mathcal{P} \equiv E_{\boldsymbol{y}}[Y^n]$ is considered, $\mathcal{H} \equiv g^n(\boldsymbol{x})$, where $g(\boldsymbol{x})$ represents the so-called performance function of the model. On the other hand, in case the calculation is aimed at computing p_F, $\mathcal{H} \equiv I_g(\boldsymbol{x})$, where I_g is the indicator function which is 1 in case $g(\boldsymbol{x}) \leq 0,\ \boldsymbol{x} \in \mathbb{R}^{n_x}$, and 0 otherwise.

To infer the bounds on $\mathcal{P}$, two optimization problems need to be solved to actively search the parameter space spanned by $[\underline{F}_X(x), \overline{F}_X(x)]$. Specifically, the lower bound is obtained as:

$$\underline{\mathcal{P}} = \min_{F_X^k \in [\underline{F}_X(x), \overline{F}_X(x)]} \mathcal{P}(F_X^k), \tag{22}$$

whereas the upper bound is determined as:

$$\overline{\mathcal{P}} = \max_{F_X^k \in [\underline{F}_X(x), \overline{F}_X(x)]} \mathcal{P}(F_X^k) \tag{23}$$

Note that each realisation F_X^k drawn from this interval represents a non-Gaussian random process with auto-correlation structure as described in Eq. (10). As such, this is effectively a double-loop approach, which might entail a non-negligible computational cost to solve. The main difficulty associated with solving these optimization problems lies in the fact that the optimisation has to be performed over the infinite-dimensional space of bounded, strictly monotonically increasing functions in the interval $[0, 1]$ (i.e., càdlàg functions). Such calculation is intractable, even for the most simple cases. In this paper, it is therefore proposed to approximate these optimization problems as discrete problems. Specifically, it is aimed at solving following problems:

$$\begin{aligned} \underline{\mathcal{P}} &= \min_{\boldsymbol{F}_X \in \boldsymbol{F}_X^I} \mathcal{P}(F_X^k) \\ \overline{\mathcal{P}} &= \max_{\boldsymbol{F}_X \in \boldsymbol{F}_X^I} \mathcal{P}(F_X^k) \end{aligned} \tag{24}$$

subject to:

$$\boldsymbol{A}\boldsymbol{F}_X \leq 0 \tag{25}$$

where $\boldsymbol{F}_X = F_X(\boldsymbol{x}_s)$, with $\boldsymbol{x}_s \in \mathbb{R}^{n_s}$ representing n_s equally spaced sample points throughout the support of $[\underline{F}_X(x), \overline{F}_X(x)]$. Similarly, $\boldsymbol{F}_X^I = [\underline{F}_X(\boldsymbol{x}_s), \overline{F}_X(\boldsymbol{x}_s)] \in \mathbb{IR}^{n_s}$ represents an n_s dimensional interval vector collecting the bounds of the p-box for each sample point in the support. The inequality shown in Eq. (23) enforces the realisations drawn from the interval vector $\boldsymbol{F}_X^I$ to be strict monotonic to ensure that they represent admissible CDFs, where $\boldsymbol{A} \in \mathbb{R}^{n_s - 1 \times n_s}$ represents an upper-triangular band matrix with $A_{1,:} = [1 \ -1 \ 0 \ \ldots \ 0]$. As such, the infinite-dimensional optimisation problem is converted to a linear-inequality-constrained optimization problem over n_s variables. Finally, it can be noted that the translation mapping explained in section 3 requires the calculation of the inverse of the CDF (see e.g., Eq. 17). This is for instance required to generate the required sample paths of $x^k(t, \omega)$ to estimate

the performance function $g(\boldsymbol{x}^k(t,\omega))$. Hereto, a piece-wise cubic Hermite polynomial interpolation is performed using the Fritsch-Carlson algorithm to estimate a functional relationship between $\boldsymbol{x}_s$ and $\boldsymbol{F}_X$. This approach is selected as this allows for generating a strictly monotonic, C^1 continuous interpolation of the inverse of $\boldsymbol{F}_X(\boldsymbol{x}_s)$. For a detailed treatment of this algorithm, the reader is referred to [28].

5. Case study 1: a quarter car model

The case study represents a quarter-car model, which is a 2-DOF idealisation of the realistic dynamics of the suspension of a car. Specifically, this case study is concerned with assessing the bounds on several comfort metrics of a vehicle suspension, given a p-box process-valued base excitation. The quarter-car dynamics can be represented as a set of two ordinary differential equations:

$$m_s\ddot{x_s} + c_s(\dot{x}_s - \dot{x}_{us}) + k_s(x_s - x_{us}) = 0 \tag{26}$$

$$m_{us}\ddot{x}_{us} - c_s(\dot{x}_s - \dot{x}_{us}) - k_s(x_s - x_{us}) + c_t(\dot{x}_{us} - \dot{x}_0) + k_t(x_{us} - x_0) = 0 \tag{27}$$

with $\dot{\bullet}$ the time derivative of $\bullet$, x_{us} the displacement of the unsprung mass (i.e., the suspension components, wheel and other components directly connected to them), x_s the displacement of the sprung mass (i.e., all components resting on the suspension), m_{us} and m_s the unsprung and sprung mass of a quarter of the car, c_s and c_t respectively the damping coefficients of the suspension and tire, k_s and k_t respectively the stiffness coefficients of the suspension and tire. Finally, x_0 and $\dot{x}_0$ are the displacement and velocity in vertical direction that excite the bottom of the wheel (i.e., the road profile). The complete road profile is denoted $x_0(t)$. The dynamics of the car are simulated over a distance of 50 (m), when the car is travelling at a speed of 10 (m/s). The one dimensional spatial domain is discretized into 1000 equidistant points and the time domain is discretized into time intervals of 0.005 (s). A schematic representation of the model is given in figure 3.

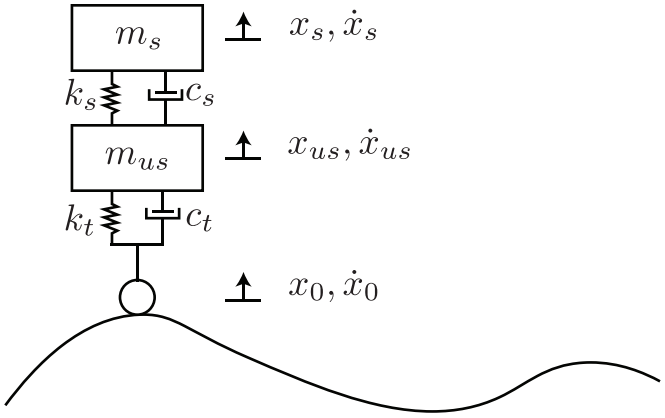

Figure 3: Schematic illustration of the quarter-car model

For the solution of this coupled system of ODEs, a state-space model is employed:

$$\frac{d}{dt}\begin{bmatrix} x_{us}-x_0 \\ \dot{x}_{us} \\ x_s - x_{us} \\ \dot{x}_s \end{bmatrix} = A \begin{bmatrix} x_{us}-x_0 \\ \dot{x}_{us} \\ x_s - x_{us} \\ \dot{x}_s \end{bmatrix} + \begin{bmatrix} -1 \\ \frac{4c_t}{m_{us}} \\ 0 \\ 0 \end{bmatrix} \dot{x}_0 \tag{28}$$

with the matrix A equal to:

$$A = \begin{bmatrix} 0 & 1 & 0 & 0 \\ \frac{-4k_t}{m_{us}} & \frac{-4(c_s+c_t)}{m_{us}} & \frac{4k_s}{m_{us}} & \frac{4c_s}{m_{us}} \\ 0 & -1 & 0 & 1 \\ 0 & \frac{4c_s}{m_s} & \frac{-4k_s}{m_s} & \frac{-4c_s}{m_s} \end{bmatrix} \tag{29}$$

Four state variables are considered, being respectively the tire deflection $(x_{us} - x_0)$; the unsprung mass velocity $\dot{x}_{us}$; the suspension stroke $x_s - x_{us}$, and sprung mass velocity $\dot{x}_s$. Typically, in the context of assessing the dynamical comfort of a car, two parameters are of interest: the suspension stroke (i.e., the relative displacement of the car body with respect to the unsprung mass) and the acceleration of the sprung mass. In the proceeding study, the damping effect of the tire, c_t is considered negligible.

Table 1: Considered case studies for the distribution free p-box process. $\mathcal{B}$ and $\mathcal{N}$ represent respectively the Beta and Normal distribution.

Case	$\underline{F}_X(x)$	$\overline{F}_X(x)$	b_t
1	$\min\left[\mathcal{B}(1,3), \mathcal{B}(5,5)\right])$	$\max\left[\mathcal{B}(1,3), \mathcal{B}(5,5)\right])$	0.5
2	$\min\left[\mathcal{B}(3,1), \mathcal{B}(5,5)\right])$	$\max\left[\mathcal{B}(3,1), \mathcal{B}(5,5)\right])$	0.5
3	$\min\left[\mathcal{B}(1,1), \mathcal{B}(2,5)\right])$	$\max\left[\mathcal{B}(1,1), \mathcal{B}(2,5)\right])$	0.5
4	$\min\left[\mathcal{B}(1,0.2), \mathcal{B}(5,5)\right])$	$\max\left[\mathcal{B}(1,.02), \mathcal{B}(5,5)\right])$	0.5
5	$\min\left[\mathcal{N}(0,0.75), \mathcal{B}(1,0.2)\right])$	$\max\left[\mathcal{N}(0,0.75), \mathcal{B}(1,0.2)\right])$	2

The complete road profile $x_0(t)$ is modelled as a p-box valued stochastic process. The auto-correlation of the underlying Gaussian process $\eta(t,\omega)$ is governed by a squared exponential auto-correlation function with a correlation length of 0.5 m. Sample path realisations of $\eta(t,\omega)$ are generated using the Karhunen–Loève series expansion, while retaining 32 terms. The stochastic content of the imprecise stochastic process is represented using via a distribution-free p-box. For illustrative reasons, the bounds of the p-box, $[\underline{F}_X(x), \overline{F}_X(x)]$ are generated by taking the extremes of a set of distributions. Hereto, 5 different case studies are considered, which are summarized in Table 1. The corresponding p-boxes area also visualized in figure 4. Each random process corresponding to a realisations of these p-boxes is given as:

$$x_0^k(t,\omega) = (F_X^k)^{-1} \circ \Phi\left(\sum_{i=1}^{n_{KL}} \sqrt{\lambda_i}\psi_i(t)\xi_i(\omega)\right) \tag{30}$$

which are generated by the optimization algorithms introduced in Section 4. Applying the double-loop optimization algorithm introduced in Section 4, the bounds on the probability of failure of the structure are computed. In this context, the performance function $g(x)$ of the car model is given as:

$$g(\boldsymbol{x}, \boldsymbol{y}) = 1 - \max_{i=1,\ldots,m} \left(\frac{|x_s(\boldsymbol{x}, t_i) - x_{us}(\boldsymbol{x}, t_i)|}{d} \right) \tag{31}$$

where the threshold value b_t is also given in Table 1. This corresponds to a first passage probability. Since the process is non-Gaussian, highly efficient and dedicated sampling methods such as Directional Importance Sampling [29], as also applied in the context of imprecise probabilities in [30] or [31], are not applicable. Therefore, the integral equation in the inner loop of the optimization is solved using Subset-∞, as presented in [32], with an initial sample size of 5000 and a proposal standard deviation of 0.1. The discretisation of $F_X(s)$, as described in Section 4, is performed using $n_s = 40$ slices, yielding a 40-dimensional optimization problem, which is solved using a gradient-free pattern search optimization algorithm. Pattern search is specifically selected to avoid the need to calculate gradients of p_F.

The results of performing the double-loop optimization problem are shown in Table 2. In this table, $\underline{p}_F^*$ and $\overline{p}_F^*$ indicate the bounds on p_F obtained by means of optimization, whereas $\underline{p}_F$ and $\overline{p}_F$ are the failure probabilities corresponding to the bounds of the p-box. As is clear, the bounds obtained by just propagating $\underline{F}_X(x)$ and $\overline{F}_X(x)$ are not conservative. This is a direct result from the fact that the car model acts as a filter on the excitation towards the responses of interest.

Table 2: Bounds on the probability of failure based on propagating the bounds, as well as performing optimization. Herein, $\underline{p}_F^*$ and $\overline{p}_F^*$ indicate the bounds on p_F obtained by means of optimization, whereas $\underline{p}_F$ and $\overline{p}_F$ are the failure probabilities corresponding to the bounds of the p-box.

Case	$\underline{p}_F$	$\overline{p}_F$	$\underline{p}_F^*$	$\overline{p}_F^*$
1	$3.25 \cdot 10^{-4}$	0.065	$2.77 \cdot 10^{-4}$	0.385
2	$3.25 \cdot 10^{-4}$	0.061	$9.95 \cdot 10^{-6}$	0.378
3	0.0045	0.400	0.0028	0.624
4	0.0038	0.469	$3.01 \cdot 10^{-4}$	0.571
5	0.0062	0.015	$9.43 \cdot 10^{-6}$	0.423

A further explanation of these results can be given based on Figure 4. This figure shows clearly that the CDF corresponding to the highest probability of failure pushes the probability mass as much as possible towards the bounds of the p-box. This makes sense from a physical standpoint since the performance function contains an absolute value operation, and hence, positive and negative responses contribute both equally to the failure. Furthermore, the considered system is a 2-degree-of-freedom oscillator where the quantity of interest is the relative displacement between the two masses. This as such constitutes a perfect symmetric system. The CDF that minimizes p_F on the other hand aims at getting as much of the probability mass as possible towards the centre of the support.

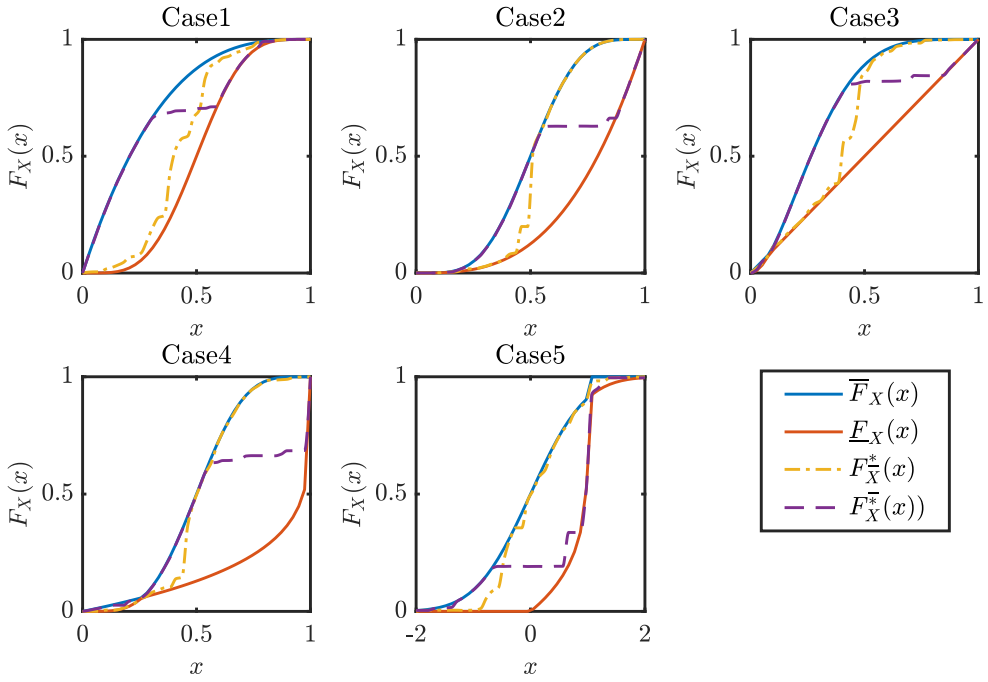

Figure 4: P-boxes corresponding to the 5 cases, as well as the realisations $F^*_{\underline{X}}$ and $F^*_{\overline{X}}$ that yield respectively $\underline{p}^*_F$ and $\overline{p}^*_F$.

6. Case study 2: an embankment settlement problem

6.1. Case introduction

As a second case study, a 2-dimensional imprecise random field is considered as the source of uncertainty in an embankment settlement problem. Hereto, a 2D Finite Element model with random Young's modulus is constructed based on the geometrical description illustrated in Figure 5 under a plain strain assumption.

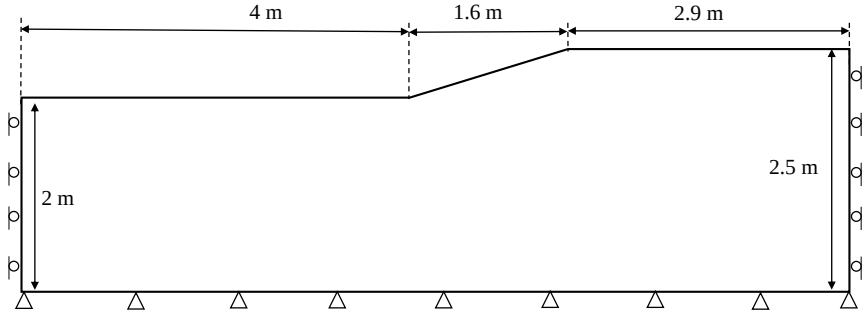

Figure 5: Schematic illustration of the embankment model

The boundary conditions of the model are that: the bottom-side is considered fully fixed, the left and right side of the geometry are free in vertical direction, and the top is free. The embankment settlement

is evaluated under self-gravity using an elastic constitutive model, which is represented as:

$$\epsilon_x = \frac{1-\nu^2}{E}(\sigma_x - \frac{\nu}{1-\nu}\sigma_y), \tag{32}$$

$$\epsilon_y = \frac{1-\nu^2}{E}(\sigma_y - \frac{\nu}{1-\nu}\sigma_x), \tag{33}$$

where ϵ and σ indicate respectively the strain and stresses in the model, E is Young's modulus and ν is the Poisson's ratio, which is set to 0.43. The earth gravity is calculated as:

$$\sigma_{eg} = \gamma - y, \tag{34}$$

where γ is the volumetric weight, which is 19.62 kg/m^3 in this model. y is the depth of the soil. This geometry is discretized into 144 quadratic rectangular finite elements with a regular size of 22.22 $\times$ 53.28 [cm]. The mesh, together with the solution of a deterministic simulation is illustrated in Figure 6. This figure in addition shows the magnitude of the displacement field u_{max}. In the ensuing analysis, the maximum vertical displacement is utilised to evaluate the embankment settlement and failure is considered when this quantity exceeds 24.4 cm.

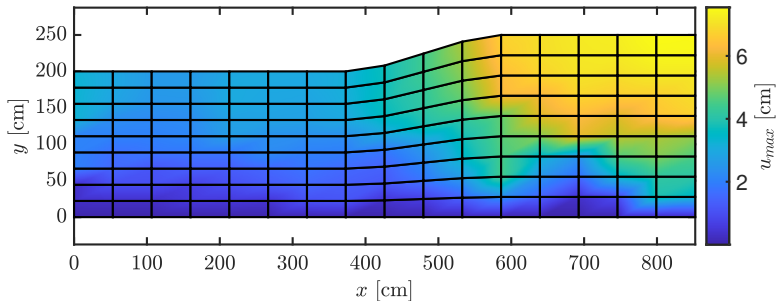

Figure 6: Finite element discretization of the geometry, together with the magnitude of the displacement fields

6.2. Imprecise random field modelling

As mentioned in the previous section, Young's modulus of the soil is modelled as an imprecise random field. The Gaussian random field $\eta(t, \omega)$ that is used as a basis for the analysis is modelled with a symmetric squared exponential kernel with correlation length of 25 [cm]. The resulting correlation function is discretized over the midpoints of the elements and the eigenvalues and eigenvectors are calculated with an iterative Krylov-Shur procedure. The truncation of the random field is selected such that 99 % of the variance is retained.

The imprecise random field is specifically defined as:

$$E(t,\omega) = 1 \cdot 10^{08} + 1 \cdot 10^{07} \cdot \left[\underline{F}_X^{-1}, \overline{F}_X^{-1}\right] \circ \Phi(\eta(t,\omega)), \tag{35}$$

where the lower and upper bound of the CDF are in this case defined as:

$$\underline{F}_X = \min\left[\mathcal{N}(0,0.5), \mathcal{N}(0,0.75)\right] \tag{36}$$

$$\overline{F}_X = \max\left[\mathcal{N}(0,0.5), \mathcal{N}(0,0.75)\right], \tag{37}$$

with $\mathcal{N}(\mu,\sigma)$ indicating a Normal distribution with mean μ and standard deviation σ. One sample of the underlying Gaussian random field $\eta(t,\omega)$, together with one realisation of the p-box random field, are shown in Figure 7.

The inverse of samples that are drawn within this p-box is calculated by fitting a piece-wise cubic Hermite polynomial to the realisation via the Fritsch-Carlson algorithm, which are generated by the optimization algorithms introduced in Section 4. Applying the double-loop optimization algorithm introduced in Section 4, the bounds on the probability of failure of the structure are computed, taking the failure criterion discussed in the previous subsection into account. Hereto, SubSet-∞ is used in the 'inner loop' with an initial sample size of 1000 samples and a proposal standard deviation for each level of $[0.1, 0.1, 0.2, 0.4, 0.5, \ldots]$. The discretization of the p-box is performed using $n_s = 50$ slices, yielding a 50-dimensional optimization problem. This optimization problem is solved using a gradient-free patternsearch optimization algorithm.

Figure 8 illustrates the realisations in the p-box that yield the best- and worst-case response in the bank settlement. The corresponding bounds on the probability of failure, consistent with the p-box are respectively $5.03 \cdot 10^{-05}$ and $2.38 \cdot 10^{-02}$. Unsurprisingly, the worst and best case behaviour in of the embankment are to be expected at the boundaries of the p-box. This is caused by the linear relation between Young's modulus and the maximum displacement in the embankment.

7. Conclusions

This paper discusses the concept of distribution-free p-box stochastic processes and processes. To generate realisations of such a process, it is proposed to pass realisations of a standard Gaussian process through an imprecisely defined translation map such that the auto-correlation of the original process is largely maintained. Furthermore, an optimization approach is introduced to actively look for those realisations inside the p-box that yield a stochastic process that yields an extreme in a probabilistic measure of a response of interest. Two case studies are included to illustrate the theoretical and computational

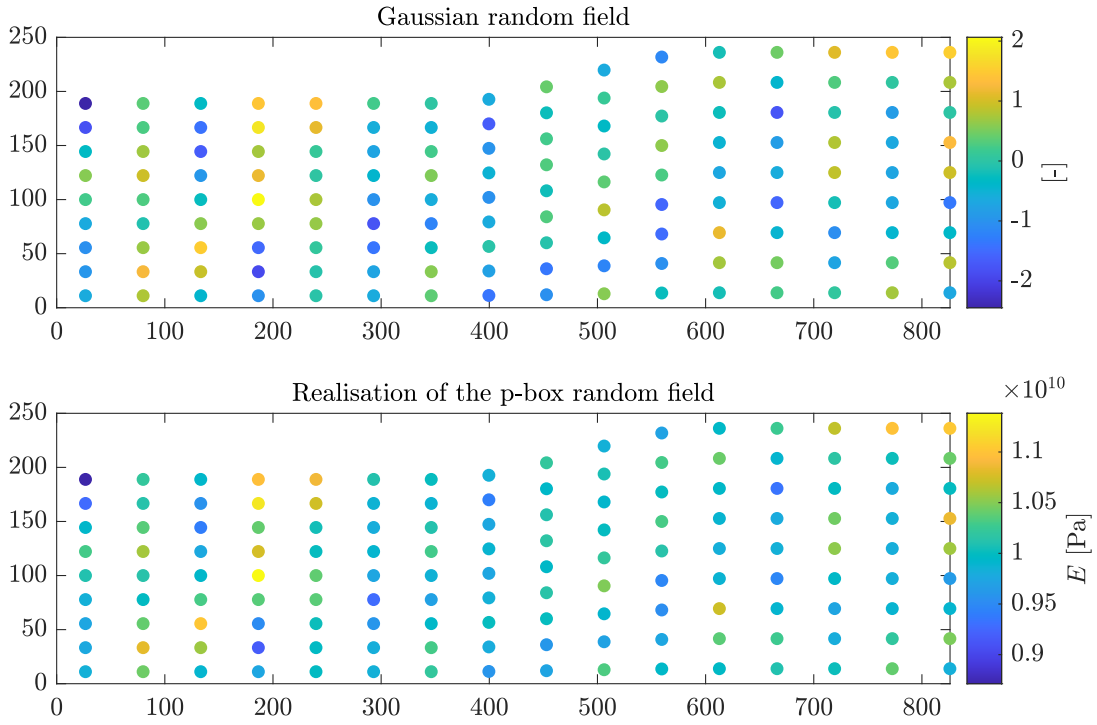

Figure 7: Top: Gaussian random field that is mapped through the interval-valued translation map. Bottom: one realisation of the resulting p-box random field.

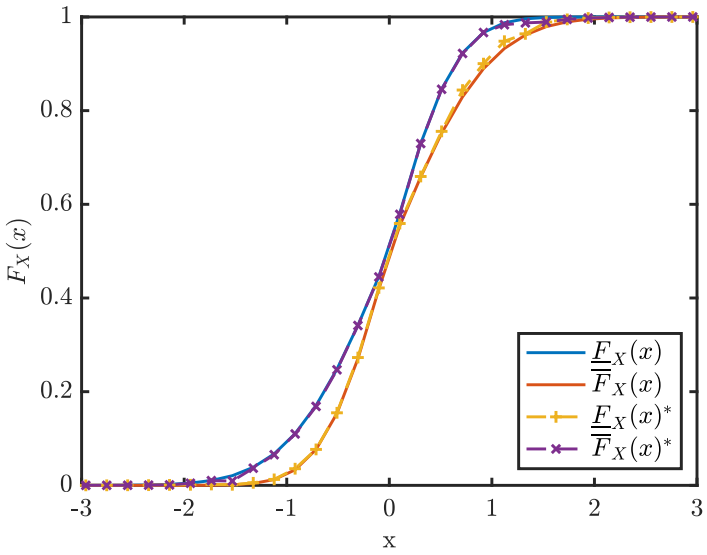

Figure 8: Imposed P-box together with the resulting realisations that yield worst and best case behaviour in the embankment.

aspects of the presented approach. The first case study on a quarter car model illustrated that the bounds of the P-box in fact do not necessarily coincide with the bounds on the probability of failure, which motivates the application of optimization algorithms. The second case study illustrates how the framework has to be applied in combination with 2-dimensional random fields in a Geotechnical case

study.

Future work will focus on propagating the p-box process such that a target auto-correlation of the p-box process can be predefined by looking for an appropriate pre-mapped auto-correlation function for each realisation F_x^k in the p-box. Furthermore, the application of more advanced approaches such as e.g., based on sparse polynomial chaos expansions as discussed in [33] to propagate the p-box will be investigated.

8. Acknowledgements

Matthias Faes acknowledges the financial support of the Research Foundation Flanders (FWO) under grant number 12P3519N as well as the Alexander von Humboldt foundation under the Humboldt Research Fellowship framework

References

[1] G. Stefanou. The stochastic finite element method: Past, present and future. Computer Methods in Applied Mechanics and Engineering, 198(9–12) (2009) 1031–1051.

[2] E. Vanmarcke, Random Fields: Analysis and Synthesis, MIT Press, Cambridge, 1983.

[3] Y. Wang, T. Zhao, K.-K. Phoon. Direct simulation of random field samples from sparsely measured geotechnical data with consideration of uncertainty in interpretation. Canadian Geotechnical Journal, 55(6) (2018), 862–880.

[4] S. Montoya-Noguera, T. Zhao, Y. Hu, Y. Wang, K.-K. Phoon. Simulation of non-stationary non-Gaussian random fields from sparse measurements using Bayesian compressive sampling and Karhunen-Loève expansion. Structural Safety, 79 (2019), 66–79.

[5] Y. Wang, T. Zhao, Y. Hu, K.-K. Phoon. Simulation of Random Fields with Trend from Sparse Measurements without Detrending. Journal of Engineering Mechanics, 145(2) (2019), 04018130.

[6] J. Ching, K.-K. Phoon. Constructing a Site-Specific Multivariate Probability Distribution Using Sparse, Incomplete, and Spatially Variable (MUSIC-X) Data. Journal of Engineering Mechanics, 146(7) (2020), 1–18.

[7] M. Beer, S. Ferson, V. Kreinovich. Imprecise probabilities in engineering analyses. Mechanical Systems and Signal Processing, 37(1–2) (2013), 4–29.

[8] P. Spanos, R. Ghanem, Stochastic finite element expansion for random media, Journal of engineering mechanics 115 (5) (1989) 1035–1053.

[9] W. Betz, I. Papaioannou, D. Straub, Numerical methods for the discretization of random fields by means of the Karhunen-Loève expansion, Computer Methods in Applied Mechanics and Engineering 271 (2014) 109–129.

[10] M. Grigoriu, Probabilistic models for stochastic elliptic partial differential equations, Journal of Computational Physics 229 (22) (2010) 8406 – 8429.

[11] S. P. Huang, S. T. Quek, K. K. Phoon, Convergence study of the truncated karhunen–loeve expansion for simulation of stochastic processes, International Journal for Numerical Methods in Engineering 52 (9) (2001) 1029–1043.

[12] H. Kim, M. D. Shields, Modeling strongly non-Gaussian non-stationary stochastic processes using the Iterative Translation Approximation Method and Karhunen-Loève expansion, Computers and Structures 161 (2015) 31–42.

[13] M.M. Dannert, A. Fau, R.M.N Fleury, M. Broggi, U. Nackenhorst, M. Beer. A probability-box approach on uncertain correlation lengths by stochastic finite element method. PAMM (Proceedings in Applied Mathematics and Mechanics), 18(1) (2018) e201800114.

[14] M. Faes, D. Moens. Imprecise random field analysis with parametrized kernel functions. Mechanical Systems and Signal Processing, 134 (2019), 106334.

[15] M. Fina, P. Weber, W. Wagner. Polymorphic uncertainty modeling for the simulation of geometric imperfections in probabilistic design of cylindrical shells. Structural Safety, 82 (2020), 101894.

[16] M.G.R. Faes, M. Daub, S. Marelli, E. Patelli, M. Beer (2021). Engineering analysis with probability boxes: a review on computational methods. Structural Safety, 93, 102092.

[17] M. Daub, S. Marelli, B. Sudret (2021), On constrained distribution-free p-boxes and their propagation, Reliable Engineering Computing 2021, Taormina, Italy.

[18] P. Walley (1997). A Bounded Derivative Model for Prior Ignorance about a Real-Valued Parameterer. Scandinavian Journal of Statistics, 24(4), pp. 463–483

[19] Kincal, C., and Koca, M.Y. 2019. Correlations of in situ modulus of deformation with elastic modulus of intact core specimens and RMR values of andesitic rocks: a case study of the Izmir subway line. Bulletin of Engineering Geology and the Environment, 78: 5281–5299.

[20] Ching J. Y., Wu, S. S. & Phoon, K. K., "Statistical Characterization of Random Field Parameters Using Frequentist and Bayesian Approaches", Canadian Geotechnical Journal 53(2), Feb 2016, 285-298

[21] M. Grigoriu, Simulation of stationary non-Gaussian translation processes, Journal of Engineering Mechanics 124 (2) (1998) 121–126.

[22] Arwade,S.R.(2004). Translation vectors with non-identically distrivuted components: application to heterogeneous materials. Proceedings, Ninth ASCE Specialty Conference on Probabilistic Mechanics and Structural Reliability, Albuquerque, New Mexico (CDROM).

[23] M. Faes, D. Moens, On auto- and cross-interdependence in interval field finite element analysis, International Journal for Numerical Methods in Engineering 121 (9) (2020) 2033–2050.

[24] M. Faes, D. Moens, Recent Trends in the Modeling and Quantification of Non-probabilistic Uncertainty, Archives of Computational Methods in Engineering 27 (3) (2020), 633–671.

[25] Verhaeghe, W.; Desmet, W.; Vandepitte, D.; Moens, D. Interval Fields to Represent Uncertainty on the Output Side of a Static FE Analysis. Computer Methods in Applied Mechanics and Engineering 2013, 260, 50–62.

[26] Jiang, C.; Ni, B. Y.; Liu, N. Y.; Han, X.; Liu, J. Interval Process Model and Non-Random Vibration Analysis. Journal of Sound and Vibration 2016, 373, 104–131.

[27] Sofi, A.; Romeo, E.; Barrera, O.; Cocks, A. An Interval Finite Element Method for the Analysis of Structures with Spatially Varying Uncertainties. Advances in Engineering Software 2019, 128 (November 2018), 1–19.

[28] F.N. Fritsch, R.E. Carlson. Monotone Piecewise Cubic Interpolation. SIAM Journal on Numerical Analysis 17(2) (1980), 238–246.

[29] M.A. Misraji, M.A. Valdebenito, H.A. Jensen, C.F. Mayorga, Application of directional importance sampling for estimation of first excursion probabilities of linear structural systems subject to stochastic Gaussian loading. Mechanical Systems and Signal Processing, 139 (2020) 106621.

[30] M.G.R. Faes, M.A. Valdebenito, D. Moens, M. Beer. Bounding the first excursion probability of linear structures subjected to imprecise stochastic loading. Computers & Structures, 239 (2020) 106320.

[31] M.G.R. Faes, M.A. Valdebenito, X. Yuan, P. Wei, M. Beer. Augmented Reliability Analysis for Estimating Imprecise First Excursion Probabilities in Stochastic Linear Dynamics (2020). Preprint Submitted to Elsevier.

[32] S.-K. Au, E. Patelli. Rare event simulation in finite-infinite dimensional space. Reliability Engineering & System Safety, 148 (2016) 67–77.

[33] R. Schöbi, B. Sudret. Uncertainty propagation of p-boxes using sparse polynomial chaos expansions. Journal of Computational Physics, 339 (2017) 307–327.

[34] Vio, R.; Andreani, P.; Tenorio, L.; Wamsteker, W. Numerical Simulation of Non-Gaussian Random Fields with Prescribed Marginal Distributions and Cross-Correlation Structure. II. Multivariate Random Fields. PUBL ASTRON SOC PAC 2002, 114 (801), 1281–1289.